PAPER

Evaluation of multi-target iridium(III)-based metallodrugs in combating antimicrobial resistance and infections caused by *Staphylococcus aureus*†

Shijie Lin,‡[a] Yushou Chen,‡[b] Yajuan Sun,‡[b] Guangying Yu,[b] Xiangwen Liao [b] and Qiang Yang [*c]

The rapid emergence and spread of multidrug-resistant bacteria pose a serious challenge to human life and health, necessitating the development of novel antibacterial agents. Herein, to address this challenge, three iridium-based antibacterial agents were prepared and their antimicrobial activity were explored. Importantly, the three complexes all showed robust potency against *S. aureus* with MIC values in the range of 1.9–7.9 µg mL^{-1}. Notably, the most active complex **Ir3** also exhibited relative stability in mammalian fluids and a significant antibacterial effect on clinically isolated drug-resistant bacteria. Mechanism studies further demonstrated that the complex **Ir3** can kill *S. aureus* by disrupting the integrity of the bacterial membrane and inducing ROS production. This multi-target advantage allows **Ir3** to not only effectively combat bacterial resistance but also efficiently clear the bacterial biofilm. In addition, when used together, complex **Ir3** could enhance the antibacterial potency of some clinical antibiotics against *S. aureus*. Moreover, both *G. mellonella* wax worms and mouse infection model demonstrated that **Ir3** has low toxicity and robust anti-infective efficacy *in vivo*. Overall, complex **Ir3** can serve as a new antibacterial agent for combating Gram-positive bacterial infections.

1 Introduction

Multidrug-resistant bacterial infections have posed a growing global health threat. The resulting death toll is anticipated to exceed that of AIDS and cancer combined by the year 2050.[1–3] As the most common Gram-positive pathogen, *Staphylococcus aureus* (*S. aureus*) colonizes in one-third of the world population and is one of the major pathogens to cause fatal infections.[4] Furthermore, *S. aureus* has evolved to achieve antibiotic resistance owing to the abuse of antibiotics, which makes the problem worse. It was reported that the evolution of methicillin-resistant *S. aureus* (MRSA), which is also known as a "super-bug", has resulted in nearly 20 000 deaths in the United States each year.[5] Worse yet, few drugs are available to fight against this notorious pathogen after it developed resistance.

Therefore, it is urgent to develop novel drugs for combating this so-called superbug.

In recent decades, metal-based agents as potential anti-tumor drugs have received extensive attention and research.[6] In addition, due to the unique photophysical and electrochemical properties, they were commonly used in biocatalysts and cell imaging to treat diseases, with a huge advantage to improve the accuracy of diagnosis and treatment.[7–9] In fact, metal-based antibacterial agents have also received extensive attention and possess huge potential to address drug-resistant bacterial infections.[10–14] It has been reported that iridium(III) complexes bearing polypyridine moieties showed obvious antibacterial activity against Gram-positive bacteria such as *S. aureus*.[15–18] Meanwhile, ruthenium-based complexes, which could disrupt the integrity of the bacterial membrane, not only exhibited robust antibacterial efficacy against Gram-positive bacteria but also effectively blocked the generation of bacterial resistance.[19]

In this work, three iridium-based antibacterial agents capable of bacterial membrane destruction and reactive oxygen species induction were designed and prepared, aiming to screen a better antibacterial metallodrug to combat multidrug-resistant bacteria. Their antibacterial potencies against *S. aureus* were evaluated through minimum inhibitory concentration. Furthermore, the antibacterial mechanism was confirmed using scanning electron microscopy, bacterial

aDepartment of Pharmacy, Hainan General Hospital (Hainan Affiliated Hospital of Hainan Medical University), Haikou, 570311, China

bJiangxi Provincial Key Laboratory of Drug Design and Evaluation, School of Pharmacy, Jiangxi Science&Technology Normal University, Nanchang, 330013, China

cDepartment of Clinical Pharmacy, Hainan Cancer Hospital, Haikou, 570100, China. E-mail: 18789551643@163.com

staining assay, and the leakage of cytoplasmic materials analyses. Next, a series of assays, including the hemolytic toxin secretion, bacterial biofilm formation and clearance, checkerboard assay and drug resistance development assay, were further performed to confirm the advantage of complex **Ir3** as a candidate metal-based antibiotic. At last, the *G. mellonella* wax worms and mouse infection model were employed to verify its toxicity and anti-infective efficacy *in vivo*.

2 Results and discussion

2.1 Synthesis, characterization and *in vitro* antibacterial activity against *S. aureus*

The synthesis routes of the three complexes are shown in Scheme 1.[20-22] Three iridium complexes were isolated with hexafluorophosphate as the counter anion. The structures of all complexes were characterized by HRMS spectrometry, ^{1}H-NMR, and ^{13}C-NMR. For the HRMS spectra, all found signals of [M-PF$_6$][+] were exactly the same as the theoretical values. In addition, the purity of the three complexes was confirmed by HPLC (ESI †).

Firstly, the minimum inhibitory concentrations (MIC) of the three iridium-based agents against *S. aureus* were assessed using a broth microdilution assay. The MIC values of **Ir1**, **Ir2** and **Ir3** against *S. aureus* were 7.8 µg mL^{−1}, 3.9 µg mL^{−1} and 1.9 µg mL^{−1}, respectively (Fig. 1). Notably, the antimicrobial potency of complex **Ir3**, which works best, is comparable to that of vancomycin, a glycopeptide antibiotic that is used as the first-
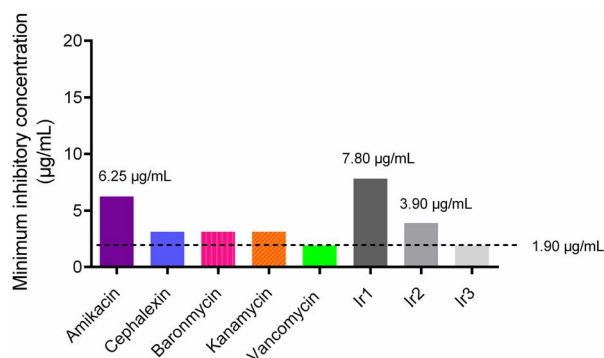

Fig. 1 Minimum inhibitory concentration (MIC) values of some antibiotics and the three iridium complexes against the *S. aureus* Newman strain.

line drug for drug-resistant *S. aureus*. In addition, complex **Ir3** exhibited robust effectiveness against drug-resistant *S. aureus* (MRSA) isolated from the clinic, with the MIC value at only 3.9 µg mL^{−1} (Table S1†).

After entering the bloodstream, metal-based agents are easily decomposed by some enzymes, which limits their clinical applications to a great extent. Therefore, the stability of the three iridium complexes was evaluated after being incubated in plasma, serum and blood at different times.[23,24] As showed in Fig. 2, the MIC values of **Ir3** remained constant after being incubated in 50% serum even for 8 h. Furthermore, the MIC values of **Ir3** only increased to 4 and 8 µg mL^{−1}
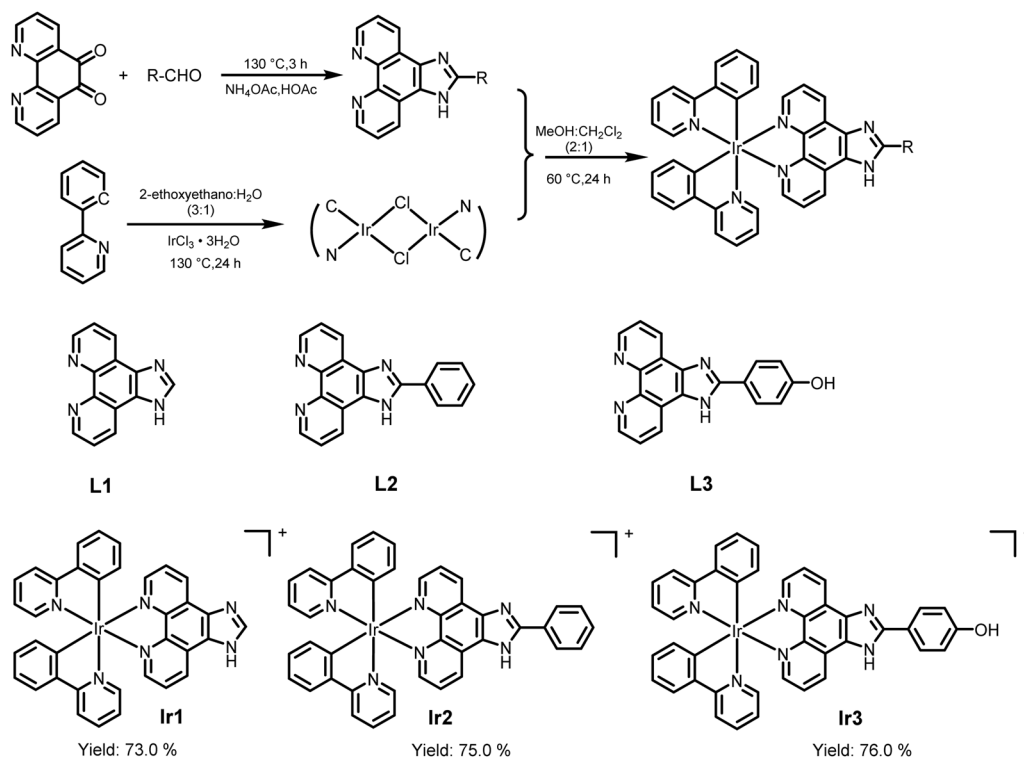
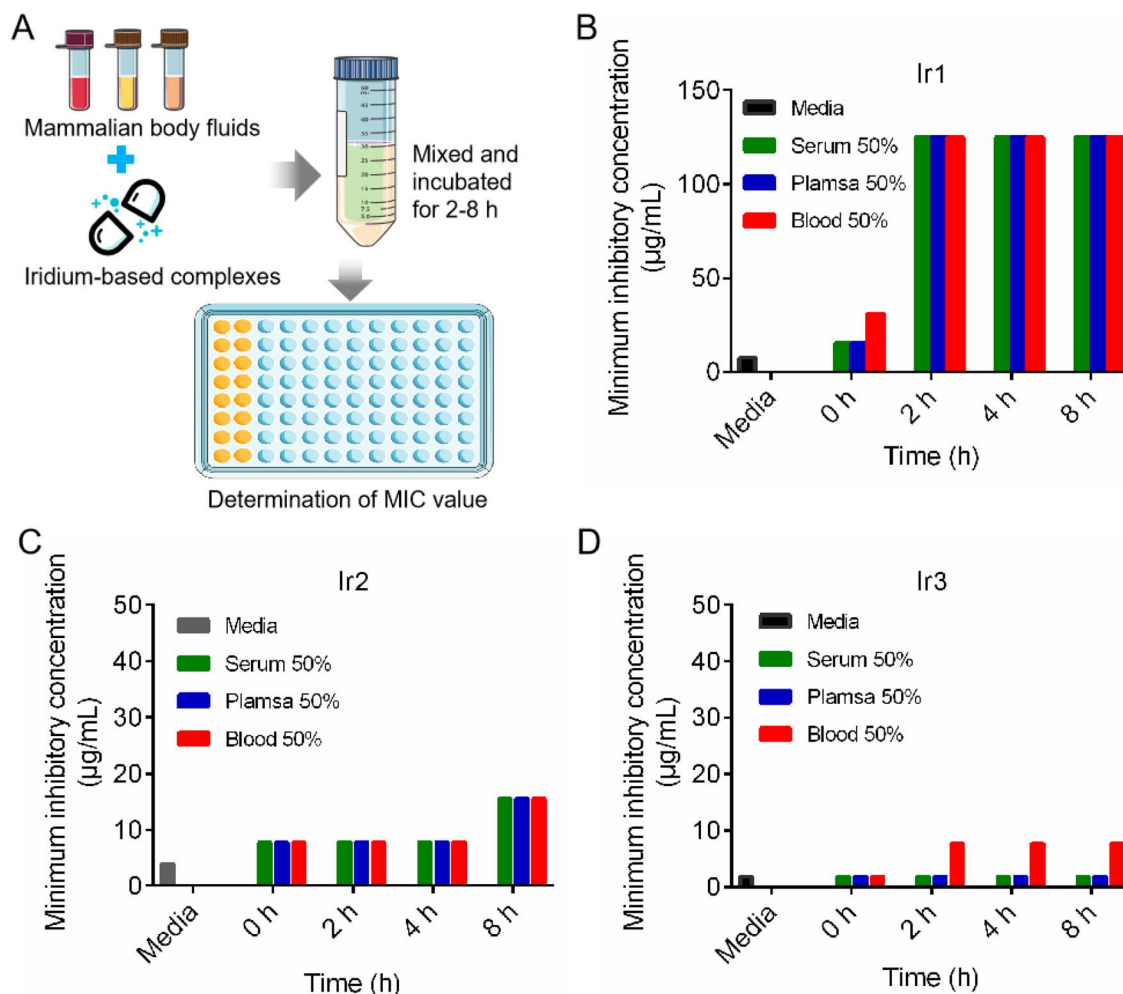**Scheme 1** The synthetic route to the iridium-based complexes and the structures of three iridium complexes.

Fig. 2 The scheme illustration of the stability evaluation of three iridium-based complexes in mammalian body fluids (A); the MIC changes of **Ir1** (B), **Ir2** (C) and **Ir3** (D) after co-incubated with mammalian body fluids.

after being incubated in blood or plasma, respectively. In contrast, the MIC values of **Ir1** and **Ir2** increased to 125 and 30 μg mL^{-1}, respectively, under the same conditions. This result indicated that **Ir3** provided the best antibacterial activity and biological stability, making it a suitable antibiotic candidate.

2.2 Antibacterial mechanism studies of Ir3

Encouraged by the excellent potency of **Ir3** against *S. aureus in vitro*, we further investigated its antibacterial mechanisms using a series of assays. At first, two fluorescence probes, PI and DAPI, were employed to investigate the damage effect on the bacterial membrane. Generally, DAPI can stain all cells blue, while PI only stained damaged cells red.[25] As shown in Fig. 3, after co-incubation with **Ir3** or vancomycin at 1 × MIC concentration for 4 h, both red and blue fluorescence signals were observed, indicating that the membrane integrity of the bacteria was compromised. In contrast, only blue fluorescence was observed in the PBS-treated group. These results indicated

that **Ir3** might effectively destroy the integrity of the bacterial cell membrane.

In general, physical destruction of the cell membrane would result in the leakage of intracellular proteins and nucleic acids. Next, the membrane-disruptive effect of complex **Ir3** on *S. aureus* was further verified by testing the leakage of cytoplasmic materials (*e.g.*, nucleic acid with absorption at 260 nm). As shown in Fig. 4A, the obvious release of nucleic acids from *S. aureus* was observed after co-incubation with complex **Ir3**. Notably, **Ir3** caused more nucleic acid leakage than polymyxin B, a small lipopeptide membrane destabilizer. Similarly, complex **Ir3** also resulted in the leakage of *ortho*-nitrophenyl-β-galactoside (ONPG), an intracellular enzyme which can produce *O*-nitrophenol with absorbance at 415 nm,[26,27] under the same condition (Fig. 4B). These results further showed that **Ir3** could significantly damage the *S. aureus* cytoplasmic membrane, leading to the leakage of cytoplasmic material. At last, the scanning electron microscope (SEM) assay was employed to directly monitor the morphological changes of the bacteria.
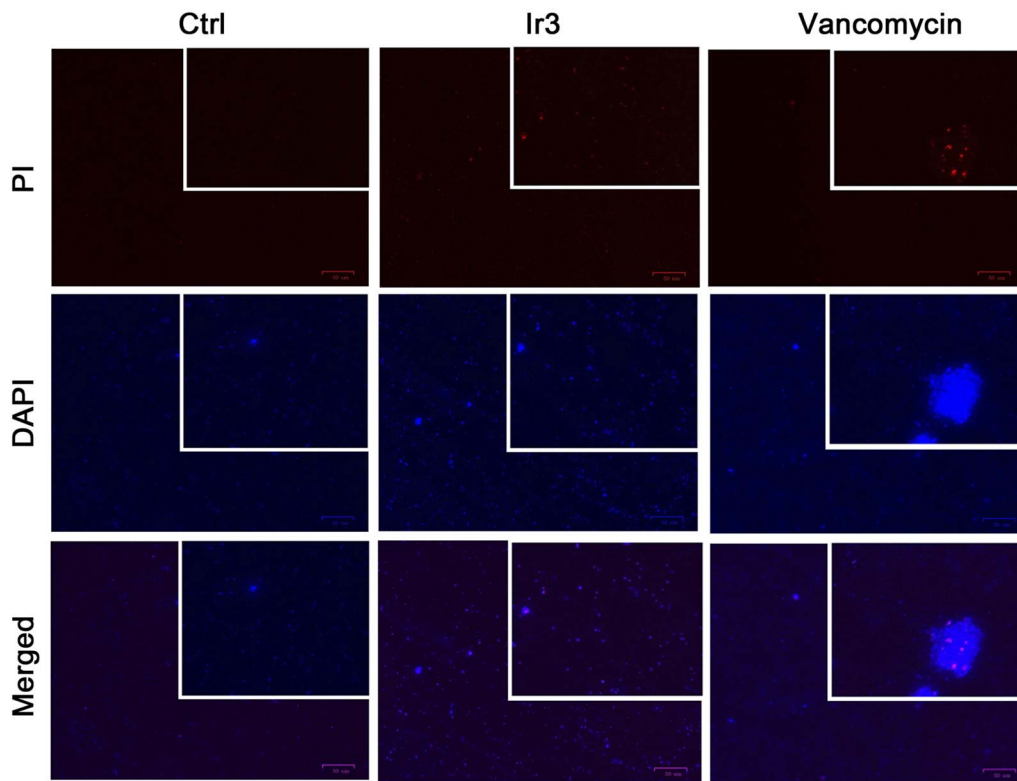
Fig. 3 Fluorescence micrographs of *S. aureus* cells stained with DAPI/PI after co-incubation with **Ir3** or vancomycin.

As shown in Fig. 4C, the morphology of the bacterial cells in the untreated group exhibits a smooth and intact membrane. However, the bacterial membrane was obviously damaged and distorted into sharp angles after co-incubation with **Ir3**. Taken together, these results suggested that complex **Ir3** can destroy the bacterial membrane, leading to bacterial death.

As is well known, many metal-based agents can induce the production of reactive oxygen species (ROS), which then kill bacteria or tumor cells. For example, some ruthenium complexes can efficiently kill pathogens by generating ROS.[28] Here, in order to verify whether **Ir3** also can induce ROS generation in *S. aureus*, we monitored the intracellular ROS levels using DCFH-DA, a green fluorescent probe which specifically recognizes ROS *in vivo*. As shown in Fig. 5A, in the presence of **Ir3**, large amounts of ROS were detected in *S. aureus*, as indicated by the obvious green fluorescence. Next, we further investigated the MIC value changes of **Ir3** in the presence of *N*-acetyl-L-cysteine (NAC), a commonly used ROS scavenger,[29] aiming to confirm the important role of ROS in **Ir3**-killed *S. aureus*. As shown in Fig. 5B, the antibacterial potency of **Ir3** against *S. aureus* was reduced by 16 times, with the MIC values increased from 1.95 to 31.25 $\mu g \ mL^{-1}$, in the presence of NAC. This result suggested that **Ir3** could cause *S. aureus* to produce ROS, which then helps **Ir3** kill them. Overall, the above series of

mechanism research experiments clearly showed that **Ir3** has a multi-target antibacterial mechanism, killing *S. aureus* by disrupting the integrity of the bacterial membrane and inducing ROS production.

2.3 Ir3 inhibited biofilm formation and eradicated the established biofilm

In vitro antibacterial activity and mechanism studies showed that complex **Ir3** has robust potency and a multi-target antibacterial mechanism. We believe this advantage must be extremely beneficial in fighting bacterial infections. As is well known, the bacterial biofilm is an important protective barrier for them against antibiotics.[30] At first, in order to identify whether **Ir3** can efficiently inhibit the formation of the *S. aureus* biofilm, a crystal violet staining assay was employed. Briefly, *S. aureus* bacteria were co-incubated with **Ir3** (0.25, 0.5 or 0.75 × MIC) at 37 °C for 48 h, then the biofilm was stained and quantified. As shown in Fig. 6A, the ability of the bacteria to produce biofilms was significantly disrupted in the presence of **Ir3**. The biofilm formation was significantly reduced by 17.4, 35.3 and 65.4% after exposure to 0.5, 1.0 and 1.5 $\mu g \ mL^{-1}$ of **Ir3**, respectively. Once the biofilm forms, bacteria can hide in it and then evade antibiotic attacks. Therefore, the ability of an
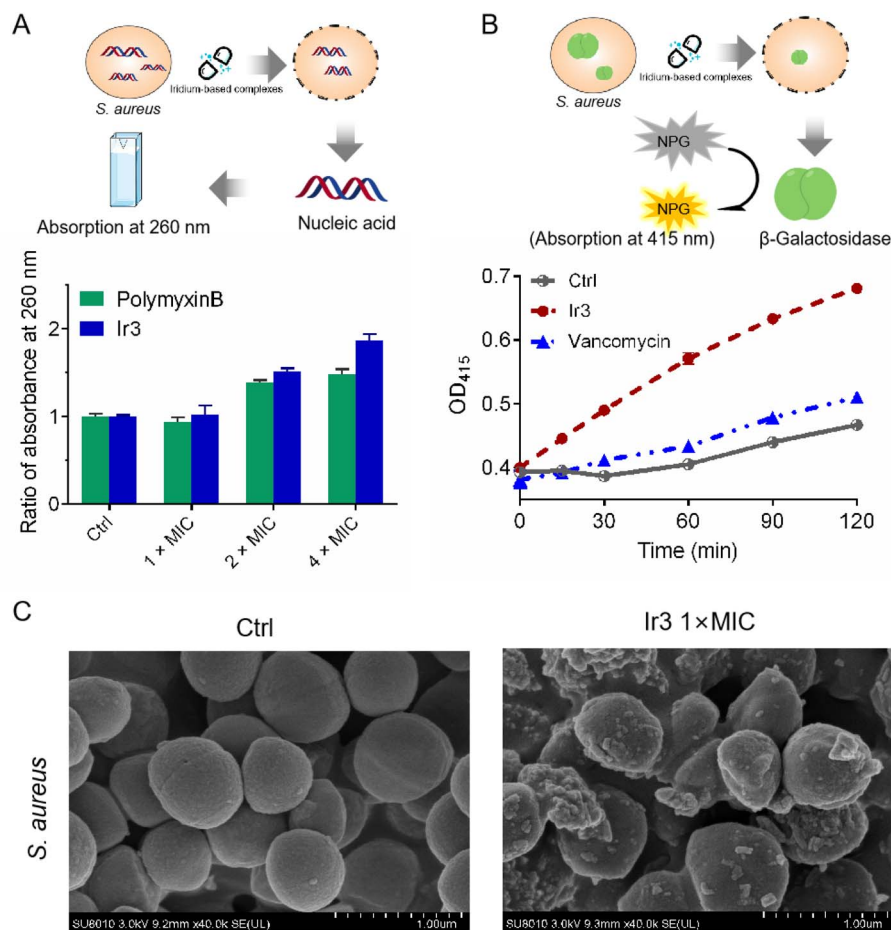
Fig. 4 (A) Ratio of the absorbance at 260 nm of the supernatant in *S. aureus* suspensions after treatment with **Ir3** or polymyxin B for 2 h at different concentrations. (B) The cytoplasmic membrane permeabilization of *S. aureus* cells treated with **Ir3** or vancomycin. (C) SEM images of *S. aureus* treated with **Ir3** at 1 × MIC.

antibacterial agent to eradicate the established biofilms is very important in its complete removal of bacteria from the site of infection.[31] Subsequently, the biofilm eradication potency of **Ir3** was investigated by monitoring the number of viable bacteria in matured biofilms after being co-incubated with it. As shown in Fig. 6B, only at 2 × MIC, **Ir3** reduced the number of viable bacteria, those hiding within the matured biofilm, by 22.2%. When the concentration of **Ir3** reached 4 × MIC, an 83.3% decrease of viable bacteria in the biofilm was observed. Taken together, these results indicated that complex **Ir3** could not only inhibit biofilm formation of *S. aureus*, but also eradicated the established biofilm.

2.4 Bacterial resistance study

One of the main drawbacks of traditional clinical antibiotics is that bacteria can easily develop resistance to them after repeated use, which poses a major challenge for the treatment of infectious diseases.[32] Since complex **Ir3** has the advantage of a multi-target mechanism and clearing matured biofilm, this should be helpful to combat bacterial resistance.

Subsequently, in order to confirm this hypothesis, the repeated use of **Ir3** against *S. aureus* was performed to induce bacterial resistance development. As showed in Fig. 7, complex **Ir3** did not induce any resistance in *S. aureus* even after 20 passages, while the MIC value of ampicillin, one of the most commonly used antibiotics in the clinic, increased by 1024 times under the same conditions. This result undoubtedly confirmed the ability of **Ir3** in fighting against the rapid development of resistance in bacteria.

2.5 Ir3 increases the susceptibility of *S. aureus* to antibiotics

As an alternative approach, in order to mitigate antibiotic resistance development, the use of antimicrobial adjuvants to increase antibiotic potency and reverse drug resistance has received much attention in recent years.[33] Next, a checkerboard assay was performed,[28] aiming to investigate whether **Ir3** can enhance the potency of the clinically used antibiotic. Here, we selected five different classes of antibiotics, including aminoglycoside antibiotic (gentamicin), macrolide antibiotics (tetracycline), polypeptide antibiotics (polymyxin
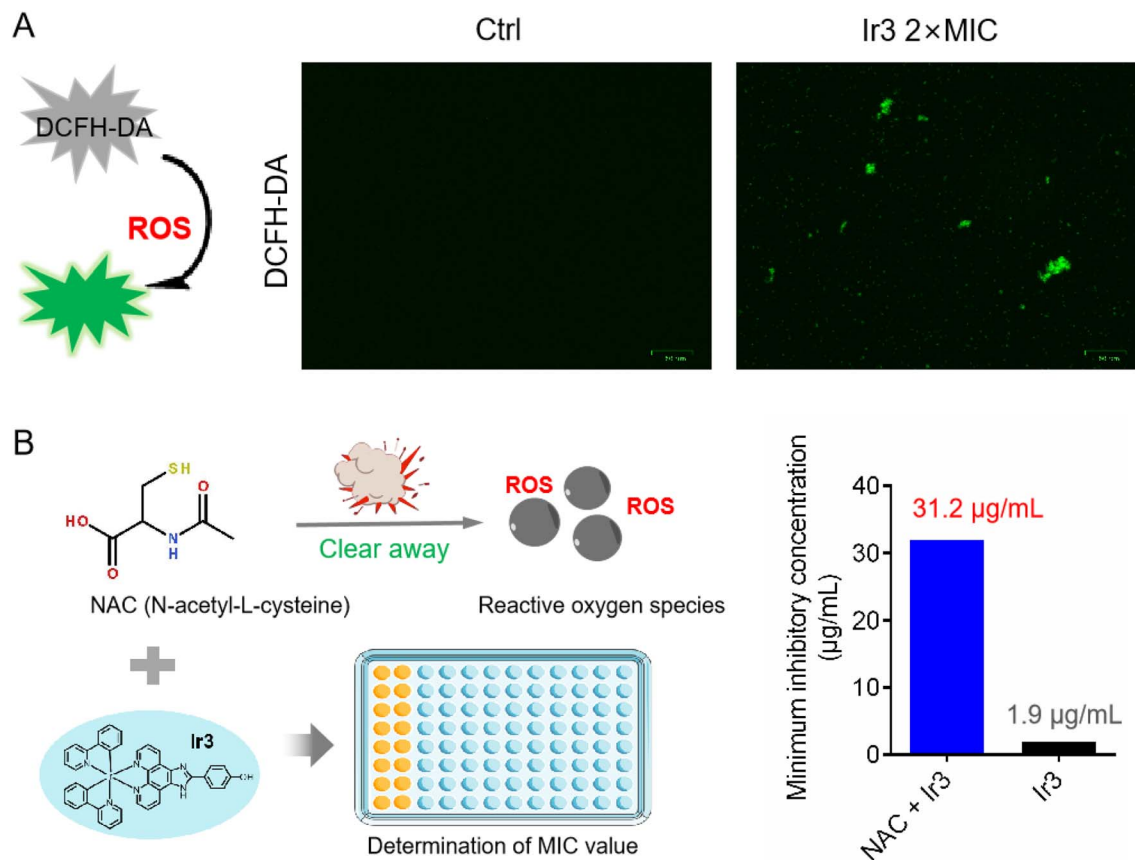
Fig. 5 (A) Minimum inhibitory concentration of **Ir3** against *S. aureus* in the presence or absence of NAC. (B) Intracellular ROS production was detected by 2,7-dichlorofluorescein diacetate (DCFH-DA), and then photographed by fluorescence microscope.
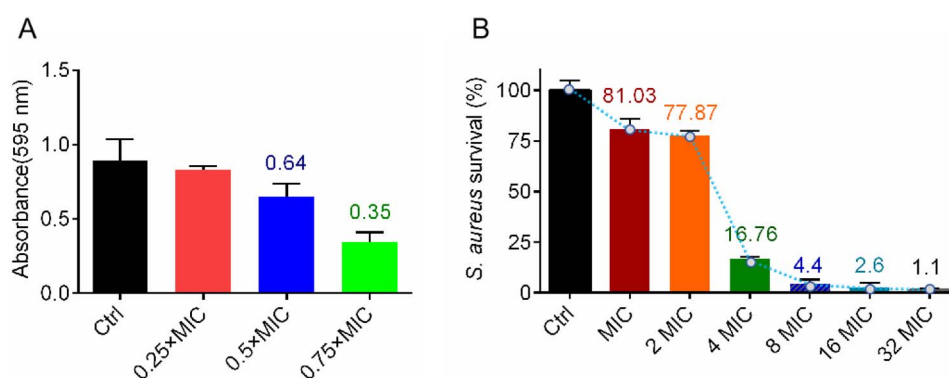

Fig. 6 (A) The formation of a *S. aureus* biofilm in the presence of **Ir3**; the biofilm was stained with crystal violet and quantified by monitoring the absorbance at 595 nm. (B) The number of viable bacteria in a matured biofilm after co-incubation with **Ir3**; all data are shown as mean ± sd.

B), glycopeptide antibiotics (vancomycin) and cephalosporins antibiotics (cefalexin). At first, the heat plots of the five checkerboard assays were drawn (Fig. 8A). Next, the fractional inhibitory concentration index (FICI), a key data to evaluate synergism, was calculated and an isobologram analysis of the synergistic effects was plotted (Fig. 8F and G). Generally, FICI ≤ 0.5 clearly suggests synergism. Our results confirmed that **Ir3** could efficiently improve the antibacterial potency of gentamicin (FICI = 0.3125), tetracycline (FICI = 0.5) and polymyxin B (FICI = 0.3125) against *S. aureus*. This result
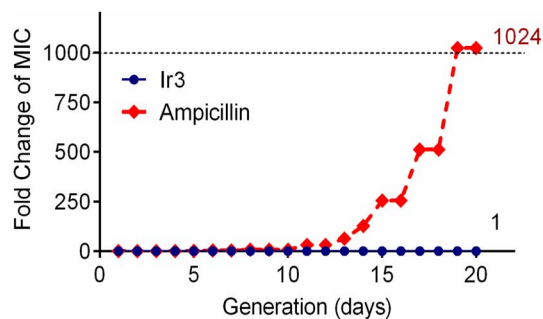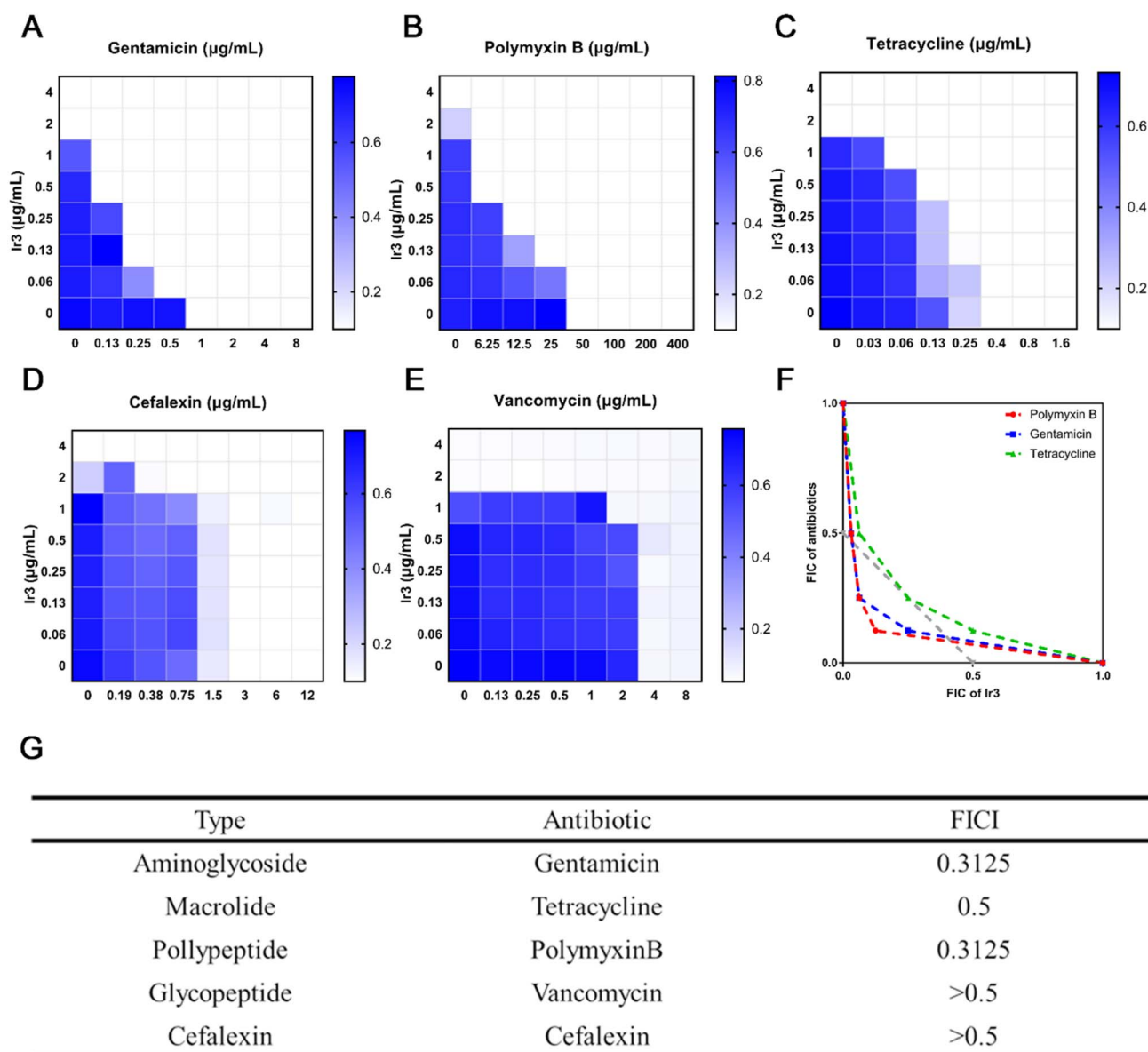
Fig. 7 Drug-resistant development profile of *S. aureus* exposed to **Ir3** and the clinically used antibiotic ampicillin.

indicated that **Ir3** had the potential as an antimicrobial adjuvant.

2.6 Ir3 can inhibit the production of hemolytic toxin of *S. aureus*

As an important bacterial exotoxin, the α-hemolysin of *S. aureus* plays an important role in its ability to cause serious infections.[34] Therefore, preventing the secretion of the hemolytic toxin from *S. aureus* is very beneficial to speed up the cure of infectious diseases. Here, to identify whether **Ir3** could inhibit the secretion of α-hemolysin from *S. aureus*, the amount of α-hemolysin was quantitatively analyzed by

Type	Antibiotic	FICI
Aminoglycoside	Gentamicin	0.3125
Macrolide	Tetracycline	0.5
Pollypeptide	PolymyxinB	0.3125
Glycopeptide	Vancomycin	>0.5
Cefalexin	Cefalexin	>0.5

$$FICI = FICI_A + FICI_B = C_A/MIC_A + C_B/MIC_B$$

Fig. 8 Heat plots of checkerboard assays for **Ir3** after combined use with some antibiotics against *S. aureus* (A–E). An isobologram analysis of the synergistic effects of **Ir3** with gentamicin, tetracycline and polymyxin B (F). Fractional inhibitory concentration indices (FICI) of antibiotics when used in combination with **Ir3** against *S. aureus* (G).
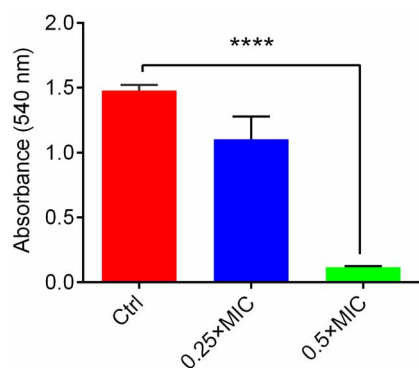
Fig. 9 The α-hemolysin secretion in *S. aureus*; the results are shown as mean ± sd.

a rabbit erythrocyte lysis test. As shown in Fig. 9, upon co-incubation with 0.5 or 1 μg mL⁻¹ of **Ir3**, the amount of α-hemolysin secretion in the bacterial culture supernatant significantly decreased by 25.4% and 99.9%, respectively. Thus, our results presented here clearly suggested that **Ir3** could efficiently inhibit the toxin production. Especially at 0.5 × MIC, the secretion of α-toxins is almost completely suppressed.

2.7 The toxicity of complex Ir3

A potential antibacterial drug should not only have robust potency, but also exhibit low toxicity to mammalian cells. This is a key prerequisite for entering clinical research. Therefore, we further explored the toxicity of complex **Ir3** *in vitro* and *in vivo*. Firstly, rabbit erythrocytes were used to
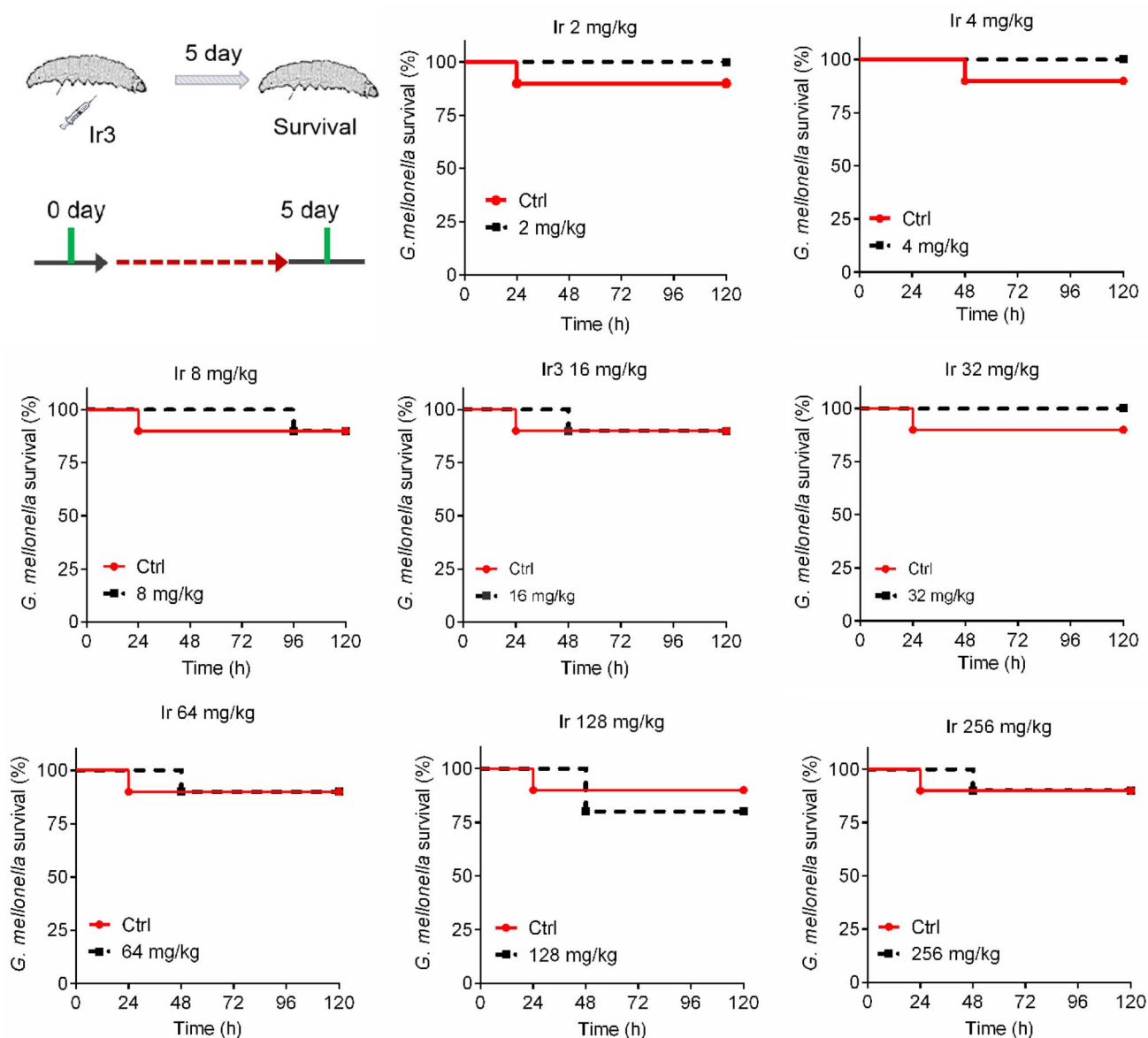

Fig. 10 The survival rate of *G. mellonella* wax worms after treatment with **Ir3** at a dose range of 8 to 256 mg kg⁻¹.
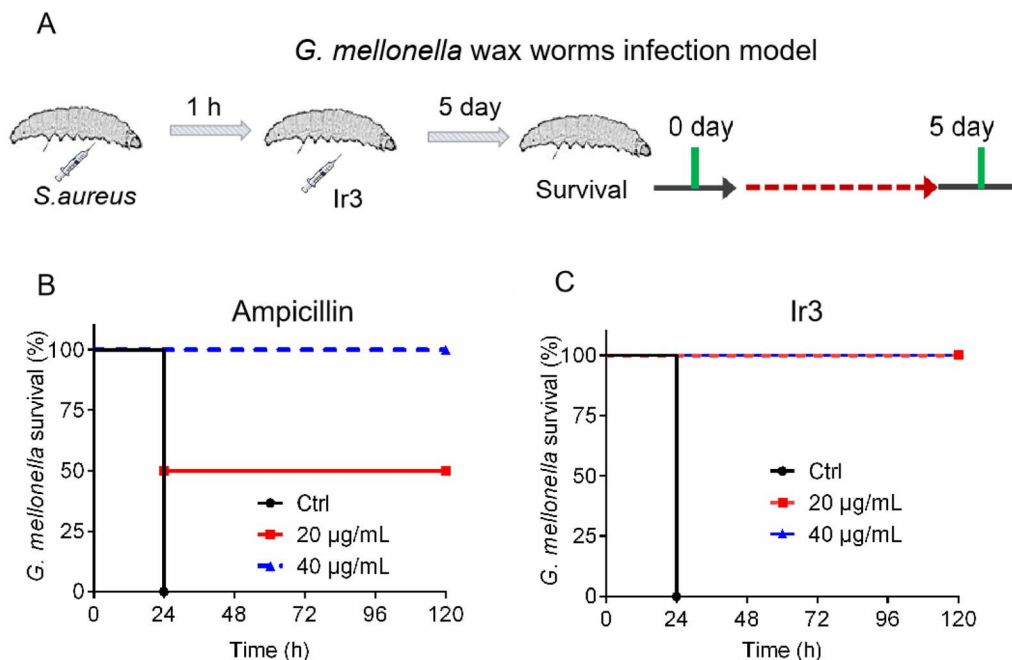
Fig. 11 (A) Schematic illustration of the experimental protocol for the *G. mellonella larva* infection model. The survival rate of *S. aureus*-infected *G. mellonella* wax worms after treatment with **Ir3** (B) or ampicillin (C).

evaluate the biocompatibility of **Ir3** *in vitro*. In brief, different concentrations of **Ir3** were incubated with rabbit erythrocytes at 37 °C. The PBS and 0.1% Triton-X treated samples were used as the negative and positive controls, respectively. At 2 μg mL^{-1} (1 × MIC), **Ir3** did not damage any red blood cells. Even at 400 μg mL^{-1} (100 × MIC), the percentage of ruptured red blood cells was only 45.0% in the presence of **Ir3**, indicating that complex **Ir3** has good blood biocompatibility (Fig. S1†). Next, to further explore the toxicity of **Ir3** *in vivo*, *G. mellonella*, an insect widely used for toxicity screening due to its significant similarity of the physiology and immune systems to those of mammals, was employed. As shown in Fig. 10, **Ir3** exhibited very low toxicity to *G. mellonella* at doses of 2 to 256 mg kg^{-1}. Even at a high dose (256 mg kg^{-1}), **Ir3** did not cause more deaths than the PBS-treated group. Taken together, our results indicated that **Ir3** has low cytotoxicity and good biocompatibility.

2.8 The therapy efficacy of Ir3 against *S. aureus*-induced infection

Due to **Ir3** presenting excellent antibacterial activity against *S. aureus in vitro* and its low toxicity, we further established two animal infection models in order to evaluate its antibacterial efficacy *in vivo*. At first, *G. mellonella* was used again. In brief, a bacterial suspension was injected into the right front gastropoda of *G. mellonella* larva. After 1 hour, **Ir3** or a commonly used clinical antibiotic (ampicillin) was injected into the left front gastropoda of the larva, and then their therapeutic effects were evaluated by recording the survival rate of the infected *G.*

mellonella within 5 days. As shown in Fig. 11, the infected *G. mellonella* all survived after treatment with 40 mg kg^{-1} **Ir3** or ampicillin. Meanwhile, at a dose of 20 mg kg^{-1}, the survival rate of the infected *G. mellonella* treated with **Ir3** was obviously higher than that with ampicillin, indicating that **Ir3** exhibited a better therapy efficacy than ampicillin, at least in the case of 20 mg kg^{-1} dose.

Next, a model of *S. aureus*-infected dermal wound was established on a mouse model to further investigate **Ir3**'s *in vivo* potency and infected-wound healing application. Briefly, the wound-infected mouse was randomly divided into 4 groups ($n = 5$), and then the *S. aureus*-infected dermal wounds were treated with a sterile cream containing **Ir3** or ampicillin. During the therapy course, the wound healing size of the mice was calculated and the mice were weighed. At last, the number of viable bacteria in the infected-wound was monitored. As shown in Fig. 12, after being treated for 10 days, marked differences in the cutaneous wound size were observed between the **Ir3**, ampicillin and PBS groups. Both **Ir3** and ampicillin significantly accelerated the healing of the wound, and the smaller wound resulting from **Ir3** suggested it has a better therapeutic effect than ampicillin at the same dose. In addition, at the dose of 150 μg mL^{-1}, the number of viable bacteria in the infected-wound of the mouse model in the **Ir3** group is less than that in the ampicillin group. It is worth noting that the weight of all of the mice did not change significantly during the treatment, again suggesting the low toxicity of **Ir3**. All in all, these results suggested that **Ir3** has excellent therapy efficacy against *S. aureus*-induced infections as well.
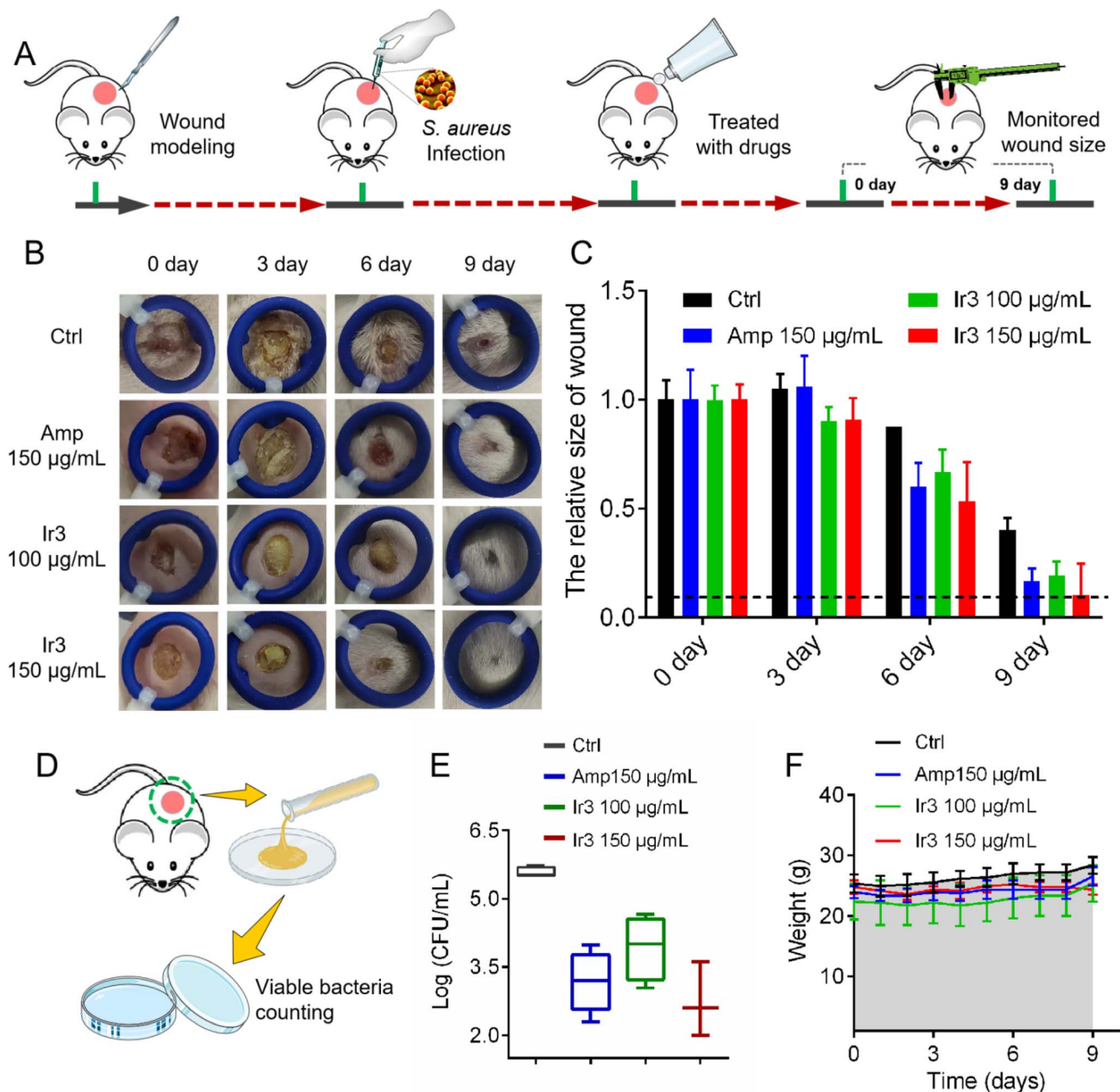
Fig. 12 (A) Schematic illustration of the experimental protocol for the mouse *S. aureus*-infected dermal wound model. (B) Representative photographs of cutaneous abscesses after treatment with **Ir3** or an ampicillin-containing ointment. (C) The relative size changes of skin ulcers over 9 days. (D) Schematic illustration of the experimental protocol for monitoring the viable bacteria in the mouse wound. (E) The number of viable bacteria in the mouse wound. (F) The relative weight changes of the mouse model over 9 days. The data are shown as mean ± sd.

3 Conclusion

In the face of a severe drug resistance situation, the development of new multi-target drugs with excellent activity that can hinder bacterial resistance is urgently needed. In this work, a series of iridium-based antibacterial agents were synthesized and evaluated. Importantly, complex **Ir3** was identified to be the most active one, which not only showed robust potency against *S. aureus* with a MIC value that only lies at 1.9 µg mL^{-1}, but also exhibited relative stability in mammalian fluids. Furthermore, using a series of assays, we demonstrated that **Ir3** has multiple targets in killing *S. aureus*. It killed bacteria mainly through disrupting the integrity of the bacterial membrane and inducing ROS production. Due to its multi-target mechanism, **Ir3** could efficiently avoid the development of bacterial resistance. The MIC values of **Ir3** against *S. aureus* did not change after being used for 20 passages. It is worth noting that **Ir3** also inhibited the biofilm formation of *S. aureus*, eradicated the established biofilm, efficiently suppressed the secretion of α-toxins, and showed potential as an antimicrobial adjuvant as it

can improve the antibacterial potency of clinical antibiotics. This series of advantages over traditional antibiotics make it a potential new metal-based antibacterial drug. In addition, using *G. mellonella* wax worms and mouse infection model, we have demonstrated that complex **Ir3** showed low toxicity and had excellent therapy efficacy against *S. aureus*-induced infection as well. Overall, our work presented here clearly suggested that iridium-based antibacterial agents possessed excellent antibacterial activity, and can serve as a novel antibacterial agents for combating Gram-positive bacterial infections.

4 Experimental section

4.1 Minimum inhibitory concentration (MIC)

Briefly, *S. aureus* cells were diluted to 1×10^6 CFU mL^{-1} with fresh TSB medium, and then transferred to a 96-well micro plate. Then, different concentrations of tested drugs were added, and the plate was incubated at 37 °C for 20 h to determinate the MIC values.

4.2 Drug resistance develop assay

The minimum inhibitory concentration (MIC) was employed to evaluate the development of bacterial resistance after exposure to **Ir3** or ampicillin. Bacterial cells under $0.5 \times$ MIC of the tested compound were employed to make a new *S. aureus* suspension for the next assay. Every passage was incubated for 20 hours with shaking at 220 rpm. The process was repeated for 20 passages and the MIC values were recorded.

4.3 Hemolytic activity study

S. aureus suspensions were diluted to 1×10^6 CFU mL^{-1}, and then different concentrations of **Ir3** were added. After being incubated with shaking at 37 °C for 10 h, the supernatant was obtained through centrifugation. The fresh sterile rabbit blood was centrifuged at 2000 rpm for 2 min, and washed with PBS 3 times to obtain pure red blood cells. The bacterial supernatant (200 μL) and red blood cells (50 μL) were added into 1 mL PBS buffer. The mixture was incubated at 37 °C for 30 min, then centrifuged at 2000 rpm for 2 min. At last, the hemolytic activity was determined through the absorption at 540 nm.

4.4 Bacterial biofilm inhibition assay

A 2 mL volume of 1×10^6 CFU mL^{-1} *S. aureus* suspension was added to a 24-well polyphenylene plate, followed by different concentrations of **Ir3**. After being incubated at 37 °C for 48 h, the planktonic bacteria were removed and then washed with PBS 3 times. The plate was dried out at room temperature. Then, 0.1% crystal violet solution was used to stain the bacterial biofilm for 15 min, and washed with PBS 3 times. Afterwards, acetic acid (50%) was used to dissolve the crystal violet attached to the biofilm. Finally, the absorbance values at 595 nm were detected.

4.5 Bacterial biofilm disruption assay

A 200 μL volume of 1×10^6 CFU mL^{-1} *S. aureus* suspension was added into a 96-well micro plate. After being incubated at 37 °C

for 48 h, the planktonic bacteria were removed and then washed with PBS 3 times. Different concentrations of **Ir3** were added, and then the plate was incubated at 37 °C for 4 h. Next, the biofilm was washed with PBS 3 times, and then 200 μL PBS was added into the 96-well micro plate. Afterwards, ultrasonication was used to treat the 96-well micro plate with the attached biofilm, making it fall off. Subsequently, 50 μL suspensions were plated on a TSB agar plate to quantity the number of viable bacteria.

4.6 Checkerboard assay

S. aureus cells were diluted to 1×10^6 CFU mL^{-1} with TSB medium, and transferred into a 96-well micro plate. After adding the diluted bacterial suspension in the presence of the mixtures of **Ir3** and the antibiotics (**Ir3** and antibiotics were continuously diluted by 2-fold dilution method), the plate containing the mixtures was incubated at 37 °C for 20 h to determine the MIC of **Ir3** and the antibiotics.

4.7 DAPI/PI fluorescence staining

The *S. aureus* suspension was centrifuged at 5000 rpm for 2 min, and washed with PBS 3 times. The bacterial cell concentration was further diluted to OD$_{600}$ = 0.4 with PBS, and then **Ir3** was added. The suspension was incubated with shaking at 37 °C for 4 h. Afterwards, 30 μL DAPI (10 μM) or 30 μL PI (10 μM) were added into the bacterial suspension, and then further incubated at room temperature in the dark for 30 min. Finally, the fluorescence of the bacteria was monitored using a fluorescence microscope.

4.8 Intracellular ROS assay

Bacterial suspensions with OD$_{600}$ = 0.4 were prepared. **Ir3** was added into the bacterial suspensions with shaking at 220 rpm at 37 °C for 2 h. Afterwards, with a constant volume of 5 mL with PBS, the oxygen fluorescent probe 2,7-dichlorodihydro-fluorescein diacetate (DCFH-DA) was used to identify the bacteria ROS level. In brief, DCFH-DA (10 μL, 30 μM) was added into the bacterial suspension for 30 min under dark conditions. Then, the fluorescence of the bacteria was monitored using a fluorescence microscope.

4.9 Membrane permeability assay

S. aureus cells were diluted with M9 minimal medium, and then incubated at 37 °C for 8 h with lactose as the sole carbon source. Next, *S. aureus* cells were centrifuged at 5000 rpm for 2 min and washed with PBS 3 times. The bacterial cell concentration was diluted to OD$_{600}$ = 0.3 with PBS, and 6 mL of the bacterial suspension was added into a test tube, followed by the addition of 300 μL ONPG (1.2 mM) to each well. Then, 10 μL of **Ir3** and vancomycin were added to the test tubes and incubated with gentle shaking at 37 °C for 2 h. The hydrolysis of ONPG to *O*-nitrophenol over time was monitored at 415 nm with a micro plate reader.

4.10   Scanning electron microscope

S. aureus suspensions were centrifuged at 5000 rpm for 2 min and washed with PBS 3 times. Bacterial cells were diluted to $OD_{600} = 0.4$ with PBS. Then, **Ir3** was added and further incubated with shaking at 37 °C for 2 h. After being centrifuged for 2 min at 5000 rpm, the cells were washed with PBS 3 times. Next, bacterial cells were fixed with 2.5% glutaraldehyde overnight and dehydrated with tertbutanol. Afterwards, the surface morphology of the bacterial cell membranes was observed.

4.11   *In vivo* toxicity of the Ir3

Rabbit erythrocytes were used to evaluate the bio compatibility of **Ir3** *in vitro*. In brief, different concentrations of **Ir3** were added into each well containing rabbit erythrocytes. The PBS and 0.1% Triton-X treated rabbit erythrocytes were used as the negative and positive controls, respectively. The hemolytic activity was determined through the absorbance value at 540 nm. Next, to further explore the *in vivo* toxicity of **Ir3**, *G. mellonella* was used. Prior to injection, the site was sterilized with ethanol. Then, 10 μL **Ir3** was injected into the right front gastropoda of the larva. Afterwards, the survival rate of *G. mellonella* was observed within 5 days.

4.12   Mouse Infection Model

All mouse infection models were purchased from Nanjing Kerusi Animal Co., LTD. The mouse infection models were divided into four groups (5 mice in each group), then wounds were generated on the backs of the mice. Next, *S. aureus* suspensions were diluted to $OD_{600} = 1$ with PBS, and the wounds on the mice were injected with the *S. aureus* suspension. After 24 hours of infection, the ointments containing **Ir3** or ampicillin were softly smeared on the abscess, and the size of the wounds was measured over times. Thereafter, the mice were weighed. Nine days later, the tissues were collects and the viable bacteria were counted by the surface plating method.

4.13   *G. mellonella* Experiment

S. aureus suspensions were centrifuged at 5000 rpm for 2 min and washed with PBS 3 times. Next, bacterial cells were diluted to the absorbance of $OD_{600} = 0.3$ with PBS. Prior to injection, *G. mellonella* was sterilized with ethanol. A 5 μL volume of *S. aureus* bacterial suspension was injected into the right front gastropoda of the larva. After 1 hour, a different dose of **Ir3** or ampicillin was injected into the left front gastropoda of larva. At last, the survival rate of *G. mellonella* was observed within 5 days.

Ethical statement

The animal study was reviewed and approved by the Animal Care and Use Committee of Jiangxi Science&Technology Normal University, and complied with the academic guidelines for the care and use of laboratory animals.

Author contributions

Shijie Lin: data curation, investigation, writing. Yushou Chen: formal analysis, investigation, writing. Yajuan Sun: investigation. Guangying Yu: formal analysis, methodology. Xiangwen Liao: funding acquisition, project administration, supervision. Qiang Yang: funding acquisition, project administration, supervision.

Conflicts of interest

The authors have declared that there is no conflict of interest.

Acknowledgements

References

1 Q. Kong, G. Li, F. Zhang, T. Yu, X. Chen, Q. Jiang and Y. Wang, *J. Med. Chem.*, 2022, **65**, 11309–11321.

2 A. R. Collaborators, *Lancet*, 2022, **399**, 629–655.

3 H. Fongang, A. T. Mbaveng and V. Kuete, *Adv. Bot. Res.*, 2023, **106**, 1–20.

4 Y. Jiang, M. Han, Y. Bo, Y. Feng, W. Li, J. R. Wu, Z. Song, Z. Zhao, Z. Tan, Y. Chen, T. Xue, Z. Fu, S. H. Kuo, G. W. Lau, E. Luijten and J. Cheng, *ACS Cent. Sci.*, 2020, **6**, 2267–2276.

5 H. Y. Chow, K. H. L. Po, P. Gao, P. Blasco, X. Wang, C. Li, L. Ye, K. Jin, K. Chen, E. W. C. Chan, X. You, R. Yi Tsun Kao, S. Chen and X. Li, *J. Med. Chem.*, 2020, **63**, 3161–3171.

6 C. Licona, J. B. Delhorme, G. Riegel, V. Vidimar, R. Cerón-Camacho, B. Boff, A. Venkatasamy, C. Tomasetto, P. Gomes, D. Rognan, J. N. Freund, R. Lagadec, M. Pfeffer, I. Gross, G. Mellitzer and C. Gaiddon, *Inorg. Chem. Front.*, 2020, **7**, 678–688.

7 E. Baggaley, J. A. Weinstein and J. A. G. Williams, *Coord. Chem. Rev.*, 2012, **256**, 1762–1785.

8 A. Pothig and A. Casini, *Theranostics*, 2019, **9**, 3150–3169.

9 B. M. Zeglis, V. C. Pierre and J. K. Barton, *Chem. Commun.*, 2007, **44**, 4565–4579.

10 E. A. Kukushkina, S. I. Hossain, M. C. Sportelli, N. Ditaranto, R. A. Picca and N. Cioffi, *Nanomaterials*, 2021, **11**, 1687.

11 A. Pathak, V. Blair, R. Ferrero, L. Kedzierski and P. Andrews, *J. Inorg. Biochem.*, 2017, **177**, 266–275.

12 P. Arthi, M. Dharmasivam, B. Kaya and A. K. Rahiman, *Chem.-Biol. Interact.*, 2023, **373**, 110349.

13 A. Gupta, P. Prasad, S. Gupta and P. K. Sasmal, *ACS Appl. Mater. Interfaces*, 2020, **12**, 35967–35976.

14 A. Frei, A. Verderosa, A. Elliott, J. Zuegg and M. Blaskovich, *Nat. Rev. Chem*, 2023, **7**, 202–224.

15 C. M. Bernier, C. M. DuChane, J. S. Martinez, J. O. Falkinham and J. S. Merola, *Organometallics*, 2021, **40**, 670–1681.

16 B. F. Hohlfeld, B. Gitter, C. J. Kingsbury, K. J. Flanagan, D. Steen, G. D. Wieland, N. Kulak, M. O. Senge and A. Wiehe, *Chemistry*, 2021, **27**, 6440–6459.

17 N. Kavitha, V. Thamilarasan and N. Sengottuvelan, *J. Organomet. Chem.*, 2021, **952**, 122032.

18 L. Lu, L. Liu, W. Chao, H. Zhong, M. Wang, X. Chen, J. Lu, R. Li, D. Ma and C. Leung, *Sci. Rep.*, 2015, **5**, 14544.

19 L. Wang, L. Liu, X. Wang, Y. Tan, X. Duan, C. Zhang, J. Cheng, Y. Xiong, G. Jiang, J. Wang and X. Liao, *Eur. J. Med. Chem.*, 2022, **238**, 114485.

20 W. Zhang, F. Du, M. He, L. Bai, Y. Gu, L. Yang and Y. Liu, *Eur. J. Med. Chem.*, 2019, **178**, 390–400.

21 J. Wang, X. Hou, H. Bo and Q. Chen, *Inorg. Chem. Commun.*, 2015, **61**, 31–34.

22 L. He, M. F. Zhang, Z. Pan, K. Wang, Z. Zhao, Y. Li and Z. Mao, *Chem. Commun.*, 2019, **55**, 10472–10475.

23 H. Li, Y. Li, Y. Wang, L. Liu, H. Dong and T. Satoh, *Acta Biomater.*, 2022, **142**, 136–148.

24 H. Li, S. Fu, L. Liu, X. Yuan, Y. Wang, C. Zhang, H. Dong and T. Satoh, *Eur. J. Med. Chem.*, 2022, **228**, 113977.

25 Y. Guo, E. Hou, T. Wen, X. Yan, M. Han, L. P. Bai, X. Fu, J. Liu and S. Qin, *J. Med. Chem.*, 2021, **64**, 12903–12916.

26 L. Chopra, G. Singh, K. Kumar Jena and D. K. Sahoo, *Sci. Rep.*, 2015, **5**, 13412.

27 R. Kuppala, M. Govindarajan, R. Tambat, N. Patel, H. Nandanwar, K. Bhutani and K. Kartha, *RSC Adv.*, 2016, **6**, 3700–3713.

28 C. Zhang, R. Yu, L. Wang, H. Huang, J. Wang, X. Liao, X. Duan and Y. Xiong, *Eur. J. Med. Chem.*, 2022, **240**, 114562.

29 A. I. Rodriguez-Rosado, E. Y. Valencia, A. Rodriguez-Rojas, C. Costas, R. S. Galhardo, J. Rodriguez-Beltran and J. Blazquez, *J. Antimicrob. Chemother.*, 2019, **74**, 2188–2196.

30 F. Chen, J. Moat, D. McFeely, G. Clarkson, I. J. Hands-Portman, J. P. Furner-Pardoe, F. Harrison, C. G. Dowson and P. J. Sadler, *J. Med. Chem.*, 2018, **61**, 7330–7344.

31 W. Chang, J. Liu, M. Zhang, H. Shi, S. Zheng, X. Jin, Y. Gao, S. Wang, A. Ji and H. Lou, *Nat. Commun.*, 2018, **9**, 5102.

32 K. O'Connell, J. Hodgkinson, H. Sore, M. Welch, G. Salmond and D. Spring, *Angew. Chem., Int. Ed.*, 2013, **52**, 10706–10733.

33 X. Ding, C. Yang, W. Moreira, P. Yuan, B. Periaswamy, P. de Sessions, H. Zhao, J. Tan, A. Lee, K. X. Ong, N. Park, Z. C. Liang, J. Hedrick and Y. Yang, *Adv. Sci.*, 2020, **7**, 2001374.

34 A. Steinhuber, R. Landmann, C. Goerke, C. Wolz and U. Fluckiger, *Int. J. Med. Microbiol.*, 2008, **298**, 599–605.